Graphical Abstract

Transformed-FNV: wave forces on a vertical cylinder – a free-surface formulation

P. H. Taylor, T. Tang, T. A. A. Adcock, J. Zang

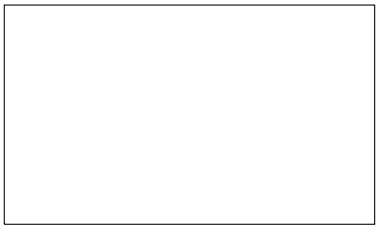

Highlights

Transformed-FNV: wave forces on a vertical cylinder – a free-surface formulation

P. H. Taylor, T. Tang, T. A. A. Adcock, J. Zang

- We propose a novel transformation of the well-known FNV theory that expresses the total force on a vertical cylinder solely in terms of the fully nonlinear wave kinematics at the free surface.
- We further propose a fully approximated version of T-FNV that uses only the nonlinear free-surface elevation time history at the position of the column.
- The new T-FNV formulations also show the increased role of higher harmonics in force time histories compared to the harmonics in the free-surface displacements.

Transformed-FNV: wave forces on a vertical cylinder – a free-surface formulation

P. H. Taylor[c], T. Tang[a], T. A. A. Adcock[a], J. Zang[b]

[a] *Department of Engineering Science, University of Oxford,, Oxford, UK*
[b] *Department of Architecture & Civil Engineering, University of Bath, Bath, UK*
[c] *Oceans Graduate School, The University of Western Australia, Perth, Western Australia*

Abstract

Existing force models for a vertical surface-piercing cylinder require water depth integration from the seabed to the free surface to determine the total inline force. However, acquiring the full wave kinematics profiles beneath the water surface presents a significant computational task. We revisit the finite water depth version of the well-known FNV theory (Kristiansen & Faltinsen, 2017, Journal of Fluid Mechanics, 833, 773–805) and propose a transformed version that expresses the total force solely in terms of the fully nonlinear wave properties at the free surface. This novel Transformed-FNV (T-FNV) formulation treats the Morison inertia term exactly and approximates the remaining two convective-derivative type terms with an assumption of slowly varying kinetic energy type terms. We evaluate the accuracy of this transformation against the original formulation, using wave kinematics obtained from fully nonlinear numerical simulations. Two T-FNV formulations are proposed with different input properties required. The first formulation uses the fully nonlinear wave kinematic properties at the free surface, whereas a fully approximated T-FNV formulation requires only the nonlinear free-surface elevation time history measured or calculated at the position of the column but in its absence. Both T-FNV formulations demonstrate good accuracy for wave forces for both deep and shallow-water cases against the original FNV model. The new T-FNV formulations also show the increased role of higher harmonics in the predicted force time histories when compared to those in the free-surface displacement, and the importance of using accurate higher order harmonic wave profiles in nonlinear force calculations.

Keywords: Ocean Engineering, Wave-structure interaction, Wave force,

1. Introduction

The classical fluid mechanics problem of wave loading on a vertical cylinder is of considerable practical interest at present due to the widespread use of monopiles as the supports for offshore wind turbines. In many locations, wave loading is critical for the design of such structures, see International Electrotechnical Commission (2009) Section 7.3.5. A concern associated with wave loading is the higher harmonic forces originating from the nonlinear interactions between waves and the structure. The periods of these higher frequency forces typically coincide with the natural period of the structure, which is typically engineered to be two or three times the incident wave period. This means these higher harmonics of the wave loading in storms can potentially excite structural resonance given the low damping characteristics of common offshore wind turbine constructions, see (Malenica et al., 1995; Rainey, 1995). Thus, these nonlinear wave loads contribute both to structural fatigue (Schløer et al., 2016) and also to the ultimate limit state loads. Both of these loading regimes are critical factors for the structural safety and lifespan (Wang et al., 2021).

Numerous theoretical methods have been developed to model the nonlinear interaction between waves and vertical cylinders. Standard diffraction theory based on traditional perturbation expansions to the second order of wave steepness has been established by numerous authors, including Molin (1979), Eatock Taylor and Hung (1987), and Newman (1996). Beyond the second-order diffraction theory, a model commonly referred to as 'FNV', named after its authors, was developed to calculate the third-order wave force on a slender cylinder in deep water, assuming the incident wave amplitude is similar to the cylinder's radius (Faltinsen, Newman and Vinje, 1995). The FNV model was extended to finite water depth by Kristiansen and Faltinsen (2017), and for compact cylinders (i.e. the size of the cylinder being small when compared to the characteristic wavelength of the wave so that there is no substantial scattering of the body (Chen et al., 2018; Rainey, 1995; Faltinsen et al., 1995)), the predictions agree with experimental results (Huseby and Grue, 2000; Chen et al., 2018).

However, the standard FNV model requires knowledge of the complete wave kinematics below the water free-surface and employs depth integrals

from the sea-bed up to the moving water surface to calculate the total inline forces. The internal kinematics information required by the model is awkward to obtain, particularly for long runs of random waves. In practical applications this typically leads to further approximations for the kinematics, such as Wheeler stretching (Wheeler, 1970) as recommended in Nestegård et al. (2006). In this study, we propose a new transformed version of the FNV theory (Kristiansen and Faltinsen, 2017) for unidirectional waves on finite water depth. Our goal in developing this new formulation is to avoid the extra computations of wave kinematics within the fluid while maintaining acceptable accuracy for engineering applications. With measured fully non-linear free-surface elevations as input, the proposed method requires separation of higher order harmonics of the free-surface elevation, which can be obtained from four repeats with different wave phases (see Fitzgerald et al. (2014); Feng et al. (2020)). However, with further approximations, we show how the necessity of four-phase information can be removed. Our approximation also provides new insights into the underlying fluid mechanics.

2. Transformed-FNV

In this study, we first introduce the derivation of the transformed FNV approximation for each term in the original FNV formulation in Section 2.2 and 2.3, and provide the T-FNV formulation with fully nonlinear velocity profiles at free surface in Section 2.4. We further approximate these nonlinear velocity profiles and the FNV term in Section 2.5-2.7 and derive the T-FNV formulation with only the free-surface elevation η measured at the centre position of the cylinder with the absence of the cylinder (empty tank or no cylinder test) in Section 2.8.

2.1. Original FNV formulation

We start with the classic finite depth version of the FNV formulation:

$$F = \int_{-d}^{\eta(t)} F'(z,t)\mathrm{d}z + F^{\psi}, \tag{1}$$

where $\eta(t)$ is the free-surface elevation, d is the water depth and the distributed load components per unit length on the vertical column $F'(z,t)$ are calculated with:

$$F'(z,t) = \rho\pi R^2 \left(2\frac{\partial u}{\partial t} + u\frac{\partial u}{\partial x} + 2w\frac{\partial u}{\partial z}\right), \tag{2}$$

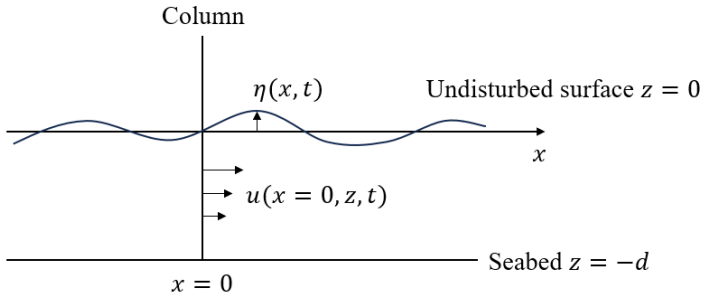

Figure 1: Schematic diagram showing the flux through a vertical line at $(x = 0)$ is connected to the motion of the free-surface for $(x > 0)$ based on the continuity condition

where (u, w) are the horizontal and vertical velocity components, R is the cylinder radius, and ρ is the fluid density. The FNV-term F^{ψ} is a point load due to the scattered potential and is applied at $z = 0$:

$$F^{\psi} = \rho\pi R^2 \frac{4}{g} u_1^2 \frac{\partial u_1}{\partial t}, \tag{3}$$

where u_1 is the linearly approximated horizontal velocity at mean water level, and g is the gravitational acceleration. Here, we calculate u_1 based on the linear contribution to u extracted from the four phase decomposition further detailed in Section 3, but we then note that this term can also be estimated from the free-surface motion directly.

2.2. $\partial u/\partial t$ term

In two-dimensional incompressible free-surface flow, the continuity condition connects the flux through a vertical line at $(x = 0)$ to the motion of the free surface for $(x > 0)$, as shown in Figure 1. Thus, we can equate the integral of horizontal velocity over the water depth to a spatial integral of the vertical velocity of the free-surface displacement downwave of the column:

$$\int_{-d}^{\eta} u(x = 0, z, t)\mathrm{d}z = \frac{\partial}{\partial t} \int_0^{\infty} \eta(x, t)\mathrm{d}x = \int_0^{\infty} \eta_t \mathrm{d}x, \tag{4}$$

where η_t is the time derivative of free-surface elevation η. The latter horizontal integral can be evaluated directly if only part of an isolated compact wave group extends to the right of the point $x = 0$. By taking the time derivative of the components in equation (4) inside the first depth integration term,

we can rewrite the depth integral of $\int_{-d}^{\eta} \frac{\partial u}{\partial t} \mathrm{d}z$ for inertia types of loading as a simple spatial integral along the fully nonlinear free surface with a local free-surface term at $x = 0$:

$$\frac{\partial}{\partial t} \int_{-d}^{\eta} u \mathrm{d}z = \int_{-d}^{\eta} \frac{\partial u}{\partial t} \mathrm{d}z + u_s \eta_t = \int_{0}^{\infty} \eta_{tt} \mathrm{d}x, \tag{5}$$

where $u_s = u(x, z = (\eta(t)))$ is the velocity in the horizontal direction at the free surface. The assumed local relationship between $\partial u/\partial t$ and the Morison inertia contribution to $F'(z, t)$ is linear but we stress that u, u_s the horizontal velocity at the free surface, and all other wave quantities are fully nonlinear here. Hence this form produces contributions to all the higher harmonics of the applied force.

For the free-surface elevation, we take the approach of a Stokes type of expansion with a narrow-banded approximation and expand the nonlinear elevation with higher order harmonics as:

$$\eta = \eta_1 + \eta_2 + \eta_3 + \cdots \tag{6}$$

where η_n is the nth order harmonics. We neglect the 2nd order difference sub-harmonic term as this is typically negligible, although the analysis could be straightforwardly extended to include this (see for instance Calvert et al. (2019)). The higher order terms can then be found as water depth dependent functions of the linear terms. Thus

$$\eta_2 = S_{22} \;\; k_p(\eta_1^2 - \eta_{1H}^2), \tag{7}$$

where subscript H denotes the Hilbert transform (Birkhoff and Kreyszig, 1984), which phase shifts all the Fourier components of a signal by 90°. Note the Hilbert transform is commonly used in signal processing, see `https://en.wikipedia.org/wiki/Hilbert_transform`. Additionally, k_p is the peak wavenumber corresponding to the spectral peak frequency of the free-surface elevation using the linear wave dispersion relation for finite water depth, and S_{22} is the usual Stokes second order coefficient (see Fenton (1990)) which converges to 1/2 for deep water. Similarly, the third order harmonic is given by:

$$\eta_3 = S_{33} \;\; k_p^2(\eta_1^3 - 3\eta_1\eta_{1H}^2), \tag{8}$$

and the third order coefficient S_{33} converges to 3/8 for deep water. The detailed formulations for the approximated higher order harmonics can be found in Walker et al. (2004).

We further express the spatial integral as an equivalent of a Fourier expansion $\times 1/\imath k$ (i.e. $\int \cdots \mathrm{d}x = \times \frac{1}{\imath k}$), where k is the appropriate wavenumber, $\imath = \sqrt{-1}$, and $1/\imath$ is effectively a Hilbert transform for sinusoidal signals. Hence the double time derivative of free-surface elevation can be written as:

$$\frac{\partial^2(\eta)}{\partial t^2} = -\omega_p^2\eta_1 - (2\omega_p)^2\eta_2 - (3\omega_p)^2\eta_3 + \cdots , \tag{9}$$

where ω_p is the spectral peak frequency of the free-surface elevation if we follow a slowly varying wave envelope approximation. We return to the choice of a characteristic frequency later. The spatial integral is now

$$\begin{aligned}\int_0^\infty \eta_{tt}\mathrm{d}x = \left\{ -\frac{\omega_p^2}{k_p}\eta_1 - \frac{(2\omega_p)^2}{(2k_p)}\eta_2 - \frac{(3\omega_p)^2}{(3k_p)}\eta_3 - \cdots \right\}_H \\ = -\frac{\omega_p^2}{k_p}\left\{\eta_1 + 2\eta_2 + 3\eta_3 + \cdots\right\}_H . \end{aligned} \tag{10}$$

Using the linear dispersion relation for finite water depth, the first water depth integral term can be expressed in known free-surface quantities at the position of the column as:

$$\int_{-d}^{\eta} \frac{\partial}{\partial t} u\mathrm{d}z = \int_0^\infty \eta_{tt}\mathrm{d}x - u_s\eta_t = -g\tanh(k_p d)\left\{\eta_1 + 2\eta_2 + 3\eta_3 + \cdots\right\}_H - u_s\eta_t, \tag{11}$$

where k_p is the wavenumber responding to the spectral peak of the free-surface spectrum. Then equation (11) captures considerable nonlinearity to all orders and replaces the vertical integral with an effective Stokes-like free-surface term comparable to the wave slope in the narrowband limit. This also shows that the higher order contributions to the force are relatively more important than those to the free surface η, which is consistent with the literature.

2.3. $u\partial u/\partial x$ and $w\partial u/\partial z$ terms

To treat the convective derivative type contributions to the distributed force, we start with the incompressible and irrotational assumptions:

$$\frac{\partial u}{\partial x} + \frac{\partial w}{\partial z} = 0 \quad \& \quad \frac{\partial u}{\partial z} - \frac{\partial w}{\partial x} = 0. \tag{12}$$

The second depth integral term can be written as:

$$u\frac{\partial u}{\partial x} = -u\frac{\partial w}{\partial z} = -\frac{\partial}{\partial z}(uw) + w\frac{\partial u}{\partial z} = -\frac{\partial}{\partial z}(uw) + w\frac{\partial w}{\partial x} \\ = -\frac{\partial}{\partial z}(uw) + \frac{1}{2}\frac{\partial}{\partial x}(w^2) \tag{13}$$

adding $\frac{1}{2}\frac{\partial}{\partial x}\tanh(k_p d)^2 \cdot u^2$ to both sides gives:

$$u\frac{\partial u}{\partial x} + \frac{1}{2}\frac{\partial}{\partial x}\tanh(k_p d)^2 \cdot u^2 = -\frac{\partial}{\partial z}(uw) + \frac{1}{2}\frac{\partial}{\partial x}\left(\tanh(k_p d)^2 \cdot u^2 + w^2\right), \tag{14}$$

For a linear wavefield and close to the free-surface where the velocity is largest, we have

$$\left.\begin{array}{ll} u \sim \coth kd & \cos\phi \\ w \sim 1 & \sin\phi \end{array}\right\}, \tag{15}$$

where ϕ is the phase. This implies that the term $((\tanh(k_p d)^2 \cdot u^2 + w^2))$ is relatively slowly varying in space, consequently it will not generate any significant 2nd sum harmonic terms. This simplification gives:

$$\frac{1}{2}\frac{\partial}{\partial x}u^2 = u\frac{\partial u}{\partial x} \approx -\frac{1}{\tanh(k_p d)^2 + 1}\frac{\partial}{\partial z}(uw). \tag{16}$$

As such, the second depth integral term can be obtained as:

$$\int_{-d}^{\eta}\left(u\frac{\partial u}{\partial x}\right)\mathrm{d}z \approx -\frac{1}{\tanh(k_p d)^2 + 1}\int_{-d}^{\eta}\frac{\partial}{\partial z}(uw)\mathrm{d}z \;\; = -\left(\frac{1}{\tanh(k_p d)^2 + 1}\right)u_s w_s, \tag{17}$$

where $w_s = w(x, z = \eta(t))$ is vertical velocity component at the free surface. This approximation shows that if we treat the wavefield as narrow-banded, one can replace the depth integrals with an effective $(\tanh(k_p d))$ term based on the peak period. We examine the accuracy of this approximation for various water depths in Section 4.2.

Finally, we investigate the last part of the water depth integral:

$$2w\frac{\partial u}{\partial z} = 2\frac{\partial}{\partial z}(uw) + 2u\frac{\partial u}{\partial x} \approx 2\frac{\partial}{\partial z}(uw) - \frac{2}{\tanh(k_p d)^2 + 1}\frac{\partial}{\partial z}(uw) = \\ \frac{2\tanh(k_p d)^2}{\tanh(k_p d)^2 + 1}\frac{\partial}{\partial z}(uw). \tag{18}$$

Therefore the last water depth integral can be expressed as:

$$\int_{-d}^{\eta}\left(2w\frac{\partial u}{\partial z}\right)\mathrm{d}z \approx \frac{2\tanh(k_p d)^2}{\tanh(k_p d)^2+1}(u_s w_s). \tag{19}$$

2.4. T-FNV formulation with fully nonlinear velocity profiles at free surface

The transformed FNV expression for the total inline force on a vertical cylinder with fully nonlinear velocities at the free surface is written as $F_{T-FNV,u}$ as:

$$F_{\text{T-FNV},u} = \int_{-d}^{\eta(t)} F'_{\text{T-FNV},u}(z,t)\mathrm{d}z + F^{\psi}_{\text{T-FNV},u}, \tag{20}$$

where the transformed FNV expression for distributed loads can be expressed without any numerical integration up the column as:

$$\begin{aligned}\int_{-d}^{\eta(t)} F'_{\text{T-FNV},u}(z,t)\mathrm{d}z &= \int_{-d}^{\eta(t)} \rho\pi R^2\left(2\frac{\partial u}{\partial t}+u\frac{\partial u}{\partial x}+2w\frac{\partial u}{\partial z}\right)\mathrm{d}z \\ &\approx \rho\pi R^2\,(\,-2g\tanh(k_p d)\,\{\eta_1+2\eta_2+3\eta_3+\cdots\}_H + \\ &\qquad \frac{2\tanh(k_p d)^2-1}{\tanh(k_p d)^2+1}u_s w_s - 2u_s\eta_t\,)\,. \end{aligned} \tag{21}$$

This gives a reasonable representation of the distributed force terms to at least 2nd order accuracy and also provides a good estimate of the higher nonlinear loading from the Morison inertia term $\int \frac{\partial u}{\partial t}\mathrm{d}z$ to orders that match the given higher order free-surface elevation results. This expression also shows the higher importance of higher-order forcing as there is an additional increasing $n-$coefficient in the front of each harmonic term in the free-surface elevation, this term looking like the time derivative of the free-surface elevation at the column.

The transformed FNV expression for FNV-term F^{ψ} can be calculated as suggested in

$$F^{\psi}_{\text{T-FNV},u} = \rho\pi R^2\frac{4}{g}u_1^2\frac{\partial u_1}{\partial t}, \tag{22}$$

where the u_1 is the horizontal velocity at the mean water level, which can be calculated using four phase decomposition method Feng et al. (2020) of the horizontal velocity profile at free-surface elevation u_s.

This version of the T-FNV is suitable for numerical simulations where the velocity profiles at the free surface are available. For experiments, where only the free-surface elevation time histories are measured, we recommend using the version of the T-FNV formulation given in Section 2.8.

2.5. Stokes expansion for the horizontal velocity at the free surface u_s

The fully nonlinear profile of horizontal velocity at the free surface is difficult to obtain during experiments. Hence, we further approximate u_s in terms of a 3rd order Stokes expansion re-written in terms of the free-surface linear elevation η_1:

$$u_{s,\text{Stokes}} = \omega_p \eta_1 \coth(k_p d) + \omega_p k_p m_2 + \frac{1}{64} \omega_p \eta_1 k_p^2 \frac{\coth(k_p d)}{\sinh^6(k_p d)} m_3, \tag{23}$$

where ω_p is the peak angular frequency based on the underlying spectrum and the two expansion terms m_2 and m_3 can be further expressed as:

$$m_2 = \eta_1^2 + \frac{3}{4}\left(\eta_1^2 - \eta_{1H}^2\right) \frac{\cosh(2k_p d)}{\sinh^4(k_p d)}, \tag{24}$$

and

$$m_3 = 8\eta_1^2 + 14\eta_{1H}^2 - \left(11\eta_1^2 + 104\eta_{1H}^2\right)\cosh(2k_p d) + 2\left(\eta_1^2 - 8\eta_{1H}^2\right)\cosh(4k_p d) + \left(\eta_1^2 - 2\eta_{1H}^2\right)\cosh(6k_p d). \tag{25}$$

This Stokes-type expression for u_s is mathematically equivalent to the standard Stokes wave theory (Stokes, 1847) , but presented in a format following linear, second order and third order terms with terms evaluated at the vertical position of the free surface. This Stokes-type expression should provide an accurate approximation up to third order in wave steepness under narrowband assumptions. We investigate the accuracy of this approximation in Section 4.3. Of course, it could be extended to 5th order if required using the form reported by Fenton (1990).

2.6. Narrowband approximation for the vertical velocity at free surface w_s

The fully nonlinear profile of vertical velocity w_s on the free surface ($x = 0, z = \eta$) is also used in the T-FNV formulation, and this is equally difficult to obtain during experiments. To approximate w_s, we start with the kinematic boundary condition at the free surface:

$$\eta_t = w_s - u_s \eta_x, \tag{26}$$

where η_x is the spatial derivative of the free-surface elevation. Unfortunately, obtaining the spatial information of free surface requires at least two wave gauges close together, rather the single one we assume elsewhere. Hence, we further approximate η_x with similar steps to those used between equation 6 and equation 11 as:

$$\eta_x = -\eta_t(k_p/\omega_p). \tag{27}$$

We note that the expression for η_x is also useful for the Rainey point load at the free surface (Rainey, 1995). Hence, the fully approximated vertical velocity at free surface w_s can be expressed in terms of the free-surface elevation and the horizontal free-surface velocity, which is also approximated in terms of η_t using equation (23), as:

$$w_s = \eta_t(1 - k_p u_{s,\text{Stokes}}/\omega_p), \tag{28}$$

and the convective derivative type contributions can be now expressed with the free surface approximation as:

$$\begin{aligned}\int_{-d}^{\eta(t)} \rho\pi R^2 \left(u\frac{\partial u}{\partial x} + 2w\frac{\partial u}{\partial z}\right) \mathrm{d}z &\approx \frac{2\tanh(k_p d)^2 - 1}{\tanh(k_p d)^2 + 1} u_s w_s \\ &\approx \frac{2\tanh(k_p d)^2 - 1}{\tanh(k_p d)^2 + 1} u_{s,\text{Stokes}} \eta_t (1 - k_p u_{s,\text{Stokes}}/\omega_p)\end{aligned} \tag{29}$$

We investigate the accuracy of this approximation in Section 4.4.

2.7. Further approximations on the FNV term F^{ψ}

The other velocity term in the original FNV formulation that requires approximation is the horizontal velocity at the mean water level (u_1) in the FNV point load previously shown in equation (2). This is due to there being no wave kinematics available at $z = 0$ when $\eta < 0$ at the structure. We approximate the FNV third order order point load as:

$$F^{\psi}_{\text{T-FNV},\eta} \approx \frac{4}{g}\ \omega_p^4\ \eta_1^2\ \eta_{1H}\ \frac{1}{\tanh^3(k_p d)} \rho\pi R^2. \tag{30}$$

Another way of approximating the linear horizontal velocity u_1 is through the four phase decomposition of $u_{s,stokes}$ in equation (23), and we present a comparison of the approximations for the FNV term in Section 4.5

2.8. T-FNV formulation with free-surface elevation only

Finally, we present the complete version of the T-FNV formulation written in terms of only the free-surface elevation at the centre position of the cylinder with the absence of the cylinder (empty tank or no cylinder test):

$$\begin{aligned} F_{\text{T-FNV},\eta} &= \int_{-d}^{\eta(t)} F'_{\text{T-FNV},\eta}(z,t)\mathrm{d}z + F^{\psi}_{\text{T-FNV},\eta} \\ &\approx 2\rho\pi R^2 \left(-g\tanh(k_p d)\left\{\eta_1 + 2\eta_2 + 3\eta_3 + \cdots\right\}_H - u_{s,\text{Stokes}}\eta_t\right) \\ &+ \rho\pi R^2 \frac{2\tanh(k_p d)^2 - 1}{\tanh(k_p d)^2 + 1} u_{s,\text{Stokes}}\eta_t(1 - k_p u_{s,\text{Stokes}}/\omega_p) + F^{\psi}_{\text{T-FNV},\eta}, \end{aligned} \quad (31)$$

where the $u_{s,\text{Stokes}}$ is given in equation (23) based on the linear free-surface elevation, and η_t can be obtained through direct numerical differentiation with respect to time of the fully nonlinear free-surface elevation (η) at the position of the cylinder, and the FNV term $F^{\psi}_{\text{T-FNV},\eta}$ can be approximated:

$$F^{\psi}_{\text{T-FNV},\eta} = \rho\pi R^2 \frac{4}{g} u_1^2 \frac{\partial u_1}{\partial t}, \quad (32)$$

where u_1 is given in equation (30) based on the linear free-surface elevation and $\frac{\partial u_1}{\partial t}$ can be obtained through direct numerical differentiation of u_1 in time. We also note that the 3rd harmonic Rainey point load at the free surface, Rainey (1995), can be approximated in a comparable way.

This formulation of the FNV is suitable for experiments where the velocity field at the free surface is not measured. Higher order harmonics of the free-surface elevation are still required for the T-FNV calculations, which can be obtained through the four-phase decomposition approach, so the experimental or numerical time history of free-surface elevation should be obtained from four repeats with different wave phases (see Fitzgerald et al. (2014); Feng et al. (2020)). Although this formulation could also be used for nonlinear force predictions starting from linear free-surface elevation η_1 only, as the higher order harmonics $(\eta_2, \eta_3, \cdots)$ can be also expressed in linear free-surface elevation in Walker et al. (2004), a further paper will be presented on this to fully justify the necessary approximations required for engineering type calculations in Monte Carlo random wave simulations.

3. Numerical model

To compare the new T-FNV model predictions with the original finite water depth FNV model, we performed numerical simulations with the OceanWave3D code to obtain the wave kinematics. OceanWave3D solves the standard potential-flow water-wave equations using sigma-transformed equations and high order finite differencing, see Engsig-Karup et al. (2009).

We consider unidirectional wave groups in this study. We generate linearly dispersed wave groups by specifying initial conditions (i.e. spatial profiles of free-surface elevation and velocity potential) at the time $t = -20T_p$ before wave group linear focus, with T_p being the spectral peak period. We specify initial conditions using the second-order theory of Sharma and Dean (1981), and also include an approximate third order correction following Barratt et al. (2020). The NewWave groups are based on an underlying JONSWAP spectrum with $\gamma = 3.3$ and the detailed parameters are shown in the figure captions. Wave kinematics are extracted at the position where the crest of the wave group reaches its maximum.

In this study, we give numerical results for three water depths, corresponding to deep through to shallow water ($k_p d = 3.39, 1.19$ and 0.88, for compactness results for this shallowest case are given in the Appendix). This wide range of water depths covers both the ringing of deep-water concrete platforms, which motivated the original FNV work Faltinsen et al. (1995), and the monopiles used in shallower water as fixed offshore wind turbine foundations.

Neglecting drag, the wave load on a vertical column can be treated as a function of three arguments: the non-dimensional water depth ($k_p d$), the wave steepness ($k_p A$) and the column radius expressed as $k_p R$ or R/d. We present results for a wide range of water depths. The effect of wave steepness is captured through the Stokes expansions for each order of wave steepness and each harmonic in frequency. Froude scaling then allows us to cover the full range of waves in the practical application of the FNV theory. The final length-scale, the cylinder radius R, is simply included as R^2 as a multiplier on the predicted forces in dimensional form. This is valid so long as the cylinder is slender, in the sense of slender body theory, so there is no significant wave diffraction and scattering. Amongst many other authors, Chen et al. (2018) show in their Fig. 19a that the simple Morison inertia loading term (our model at first order) matches linear diffraction theory for $k_p R < 0.4$. For practical wind turbine applications of any version of the FNV model, we

anticipate k_pR values well below this.

The numerical resolutions used here are based on the detailed examination of the numerical behaviour and convergence of this code given in Barratt et al. (2020). For both cases reported here, we use a spatial resolution of 4.34 m (approximately 80 nodes per peak wavelength for both cases). Twenty clustered nodes are used vertically in the water column. The total simulation time is 604 s with time steps of 0.22 s (61 per peak period for both cases).

To separate the higher order force, wave and free-surface kinematics contributions, we follow the four-phase separation method of Fitzgerald et al. (2014), building on the two-phase approach of Baldock et al. (1996), to extract the higher frequency nonlinear components of wave loading. The four-phase decomposition method assumes the form of a generalised Stokes expansion. Then, we can cleanly isolate the sum-harmonics of forces as these are important for engineering applications, see Feng et al. (2020); Mj et al. (2023). The four-phase separation method is also applied to horizontal velocity at free surface u_s to obtain the linearised horizontal velocity at mean water level u_1 for equation (22).

4. Results

4.1. Exact transformation and Stokes expansion on $\partial u/\partial t$ term

We first examine the accuracy of transforming vertical integral through the water depth into a horizontal spatial integral along the fully nonlinear free surface shown in equation (5), and also the accuracy of a Stokes expansion with the narrow-banded assumption. In Figure 2 (a, b), we show the original depth-integrated FNV inertial term and the theoretically identical free-surface integral of the vertical acceleration η_{tt} on the free-surface. The differences between these two as shown in Figure 2 (c, d) arise from inaccuracies in the numerical evaluations of the depth and free-surface integrals. The remaining harmonic components are small but have minor effects on the higher-order loading, which is important for ringing-type response calculations. The differences between the free-surface integral and the assumed Stokes form shown in Figure 2 (e, f) are also relatively small.

4.2. Slow varying assumption on $u\partial u/\partial x$ and $w\partial u/\partial z$ terms

We further examine the accuracy of treating the $((\tanh(k_pd)^2 \cdot u^2 + w^2))$ as a slowly varying term and the use of wave kinematics at the free surface to approximate the depth integral. In Figure 2 $(g - l)$, we present the original

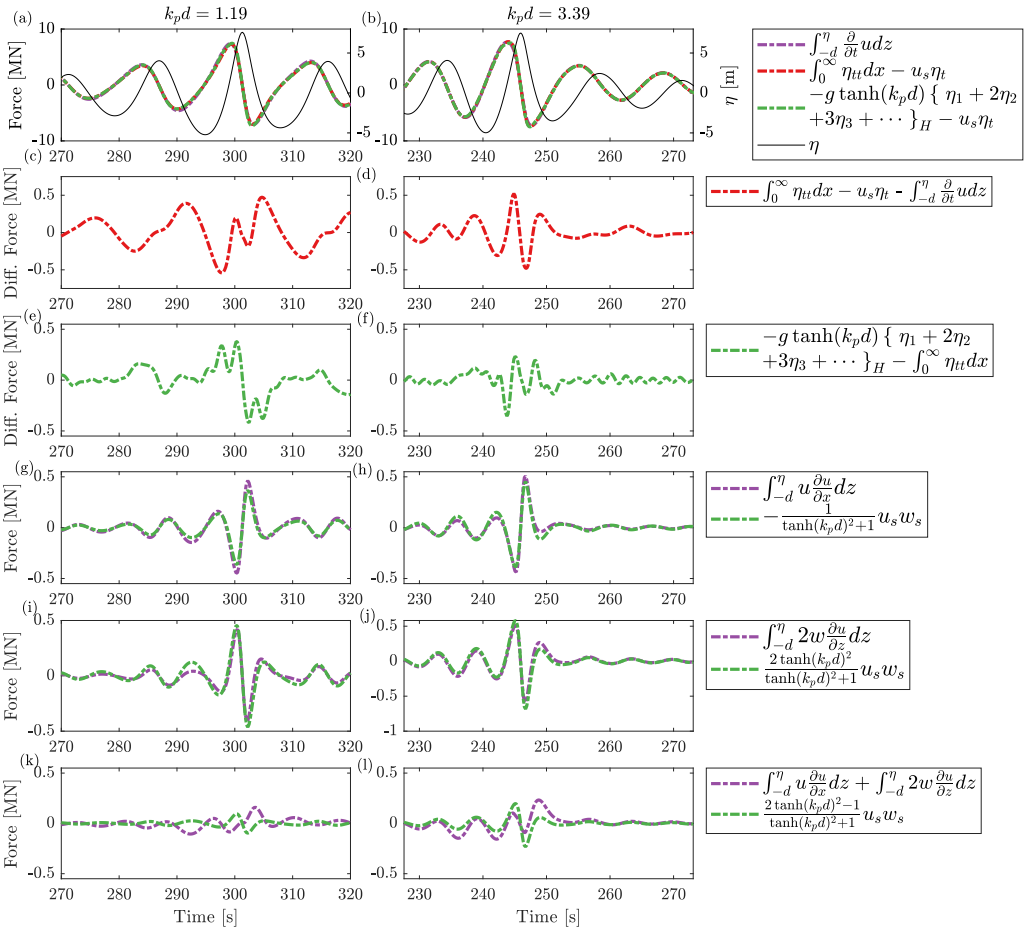

Figure 2: Comparison between all the water depth integral terms in FNV and the equivalent T-FNV formulations for $(a-d)$: the exact water depth transformation in equation (5), the thin black line shows the free-surface elevation at $(x = 0)$, $(e-f)$: Stokes Type approximation in equation (11), $(g-h)$: the first slow varying assumption in equation (17), $(i-j)$: the second slow varying assumption in equation (19) and the sum of the last two water depth integral terms in $(k-l)$. Panel (a, c, e, g, i, k) shows the case with $k_p d = 1.19$ $(k_p A = 0.17)$ and panel (b, d, f, h, j, l) shows case with $k_p d = 3.39$ $(k_p A = 0.17)$.

FNV results calculated from the depth integral (i.e. the left-hand side of the equation (17) and (19)) and the T-FNV equivalent approximation based on the kinematics at the water free surface (i.e. the right-hand side of the equation (17) and (19)). The assumption that the $((\tanh(k_p d)^2 \cdot u^2 + w^2))$ term varies slowly works better for deep water cases, but the current results also show that the approximated terms also agree reasonably well with the original FNV formulation at intermediate water depths.

From Figure 2 $(g-j)$, we also find that the last two depth integral terms $\int_{-d}^{\eta(t)} u\frac{\partial u}{\partial x}\mathrm{d}z$ and $\int_{-d}^{\eta(t)} 2w\frac{\partial u}{\partial z}\mathrm{d}z$ exhibit similar force profiles but with opposite signs. This interesting behaviour leads to the total contribution of these two terms being partially cancelled out and resulting much smaller contribution than either of these two terms individually. Indeed, the T-FNV formulation suggests the total contribution vanishes at $k_p d \approx 0.88$, which is relevant to some cases for engineering applications. As such, a crude approximation taking the depth integral part of the total inline force $-2\rho\pi R^2\ \left(g\tanh(k_p d)\left\{\eta_1 + 2\eta_2 + 3\eta_3 + \cdots\right\}_H - u_s\eta_t\right)$ can be adopted with reasonable accuracy for engineering applications.

4.3. Stokes expansion on $u_s\eta_t$ term

We now examine the accuracy of expanding the u_s term following Stokes-type expansion to the third order and the accuracy of approximating the $u_s\eta_t$ term. From Figure 3 $(a-d)$, the approximation for the u_s term and the resulting $u_s\eta_t$ term agree well with the OW3D numerical results for both deep and intermediate cases, which indicates the Stokes-type expansion to third order should provide sufficient accuracy for the T-FNV formulation.

4.4. Narrowband approximation on $u\partial u/\partial x$ and $w\partial u/\partial z$ terms

We now examine the accuracy of approximating velocity components at the free surface in both horizontal u_s and vertical direction w_s using only the free-surface elevation history for the convective derivative type contributions shown in equation (29). From Figure 3 (i,j), the narrowband approximation for w_s is accurate for both cases and we also observed a similar agreement for the approximated convective derivative type contributions shown in panel (k,l) for both intermediate and deep water cases.

4.5. Further approximations on the FNV term F^{ψ}

We now examine the accuracy of approximation for the horizontal velocity u_1 evaluated at the mean water level and also the FNV term approximation

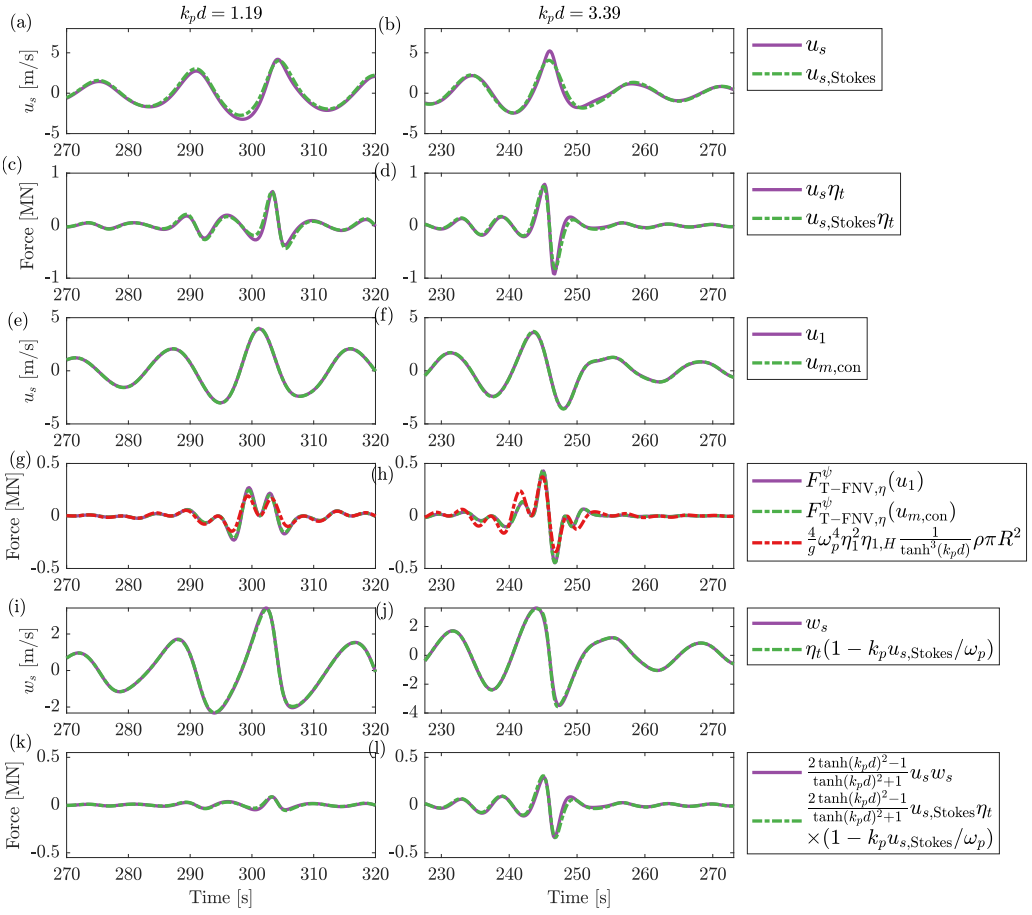

Figure 3: Comparison between velocities profiles required and the equivalent T-FNV further approximations based on free-surface elevation for $(a-b)$: the horizontal velocity profiles at the free surface required by the equation (11), $(c-d)$: the corresponding force term u_seta_t in the equation (11), $(e-f)$: the horizontal velocity at mean water level required by the FNV term F^{ψ}, $(g-h)$: the FNV term comparison between using u_1 from four phase decomposition, using full convolution from linear free-surface elevation η_1 and using narrowband approximation in equation (30). $(i-j)$: the vertical velocity profiles at the free surface approximated with equation (28), $(k-l)$: approximation for the convective derivative terms with full velocity profile at the free surface and narrowband approximation in equation (29). Panel (a, c, e, g) shows the case with $k_pd = 1.19$ $(k_pA = 0.17)$ and panel (b, d, f, h) shows case with $k_pd = 3.39$ $(k_pA = 0.17)$.

F^{ψ} proposed in Section 2.7. From Figure 3 $(e-f)$, the full calculation on the linear free-surface elevation provides an accurate prediction of the u_1, which also yields the most accurate approximation of the FNV term, as shown in Figure 3 $(g-h)$ with only very minor harmonic structure remaining. The narrowband approximation in the equation (30) also performs well, and this version can be adapted for fast predictions as the full convolution requires use of the Fourier transform.

4.6. Comparison with FNV

We now present a comparison between the total forces for the proposed T-FNV approximation and the original finite water depth FNV formulation, as shown in Figure 4 and 5. For two cases with different relative water depths, the proposed T-FNV approximation aligns closely with the original finite water depth FNV formulation. We calculate u_1 based on the linear contribution of u extracted from the four phase decomposition herein.

In the deeper relative water depth case, the T-FNV model generates an excellent match with the original FNV up to the fourth order, with only slight deviations observed at the fifth order. For the case associated with a shallower water depth, the T-FNV model tends to slightly over-predict the forces of the higher harmonics. This suggests the T-FNV model is more conservative when predicting these higher-order harmonics, which are important for the excitation of ringing-type responses. However, this mismatch between the original FNV and T-FNV for higher order harmonics can be mitigated through a single shallow water correction as a function of $k_p d$ on the characteristic wave period T_p. We further discuss this 'correction' for shallow water cases in the Appendix. The overall trends displayed in the force time histories show consistent results with the force spectral comparison.

We also present the fully approximated T-FNV based only on the free-surface elevation in time in Figure 6, where the fully approximated T-FNV model agrees well with the original formulation of FNV but is now based only on the undisturbed free-surface elevation at the cylinder. The additional black line indicates the time when the linear force reaches the maximum, which also agrees well with the expected phase shifts between linear and higher-order force harmonics described in the original 1995 FNV formulation for regular wave trains on deep water, where the maximum point of linear force should correspond to an up-zero crossing point in the second-order force and a trough in the third order force. The time histories here are based on those in Figure 2-4, 6 but with the phase of the shallow water group altered

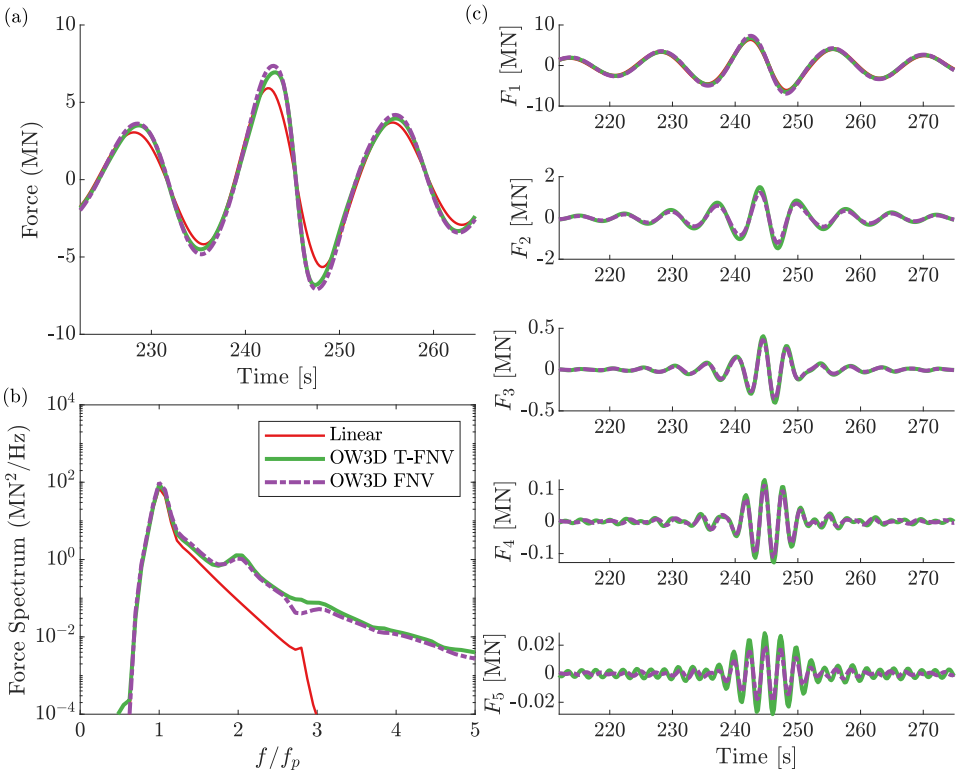

Figure 4: Comparison between the finite water depth FNV theory and the T-FNV approximations with full free-surface velocities for $k_p d = 3.39$ ($k_p A = 0.17$): total inline force, (b): force spectrum and (c): four-phase separated higher order harmonics.

such that the linear component of force achieves its maximum at net zero phase. Then, the total second harmonic is up-crossing through zero and the 3rd harmonic is at its minimum, so 180 degrees out of phase. Both for this shallow water case and for the numerical deeper water one (not shown), this relative phasing matches exactly that for the harmonics in the original FNV paper.

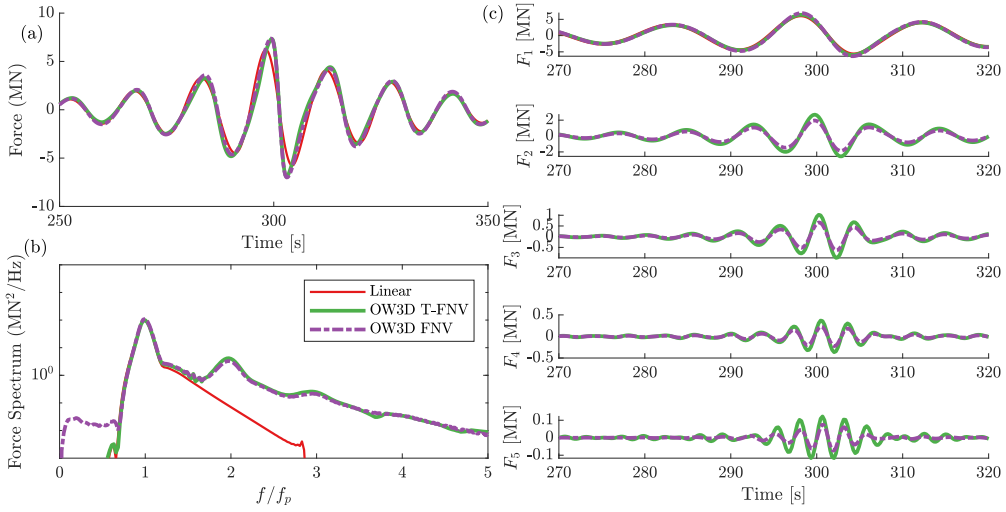

Figure 5: Comparison between the finite water depth FNV theory and the T-FNV approximations with full free-surface velocities for $k_p d = 1.19$ ($k_p A = 0.17$) (a): total inline force, (b): force spectrum and (c): four-phase separated higher order harmonics.

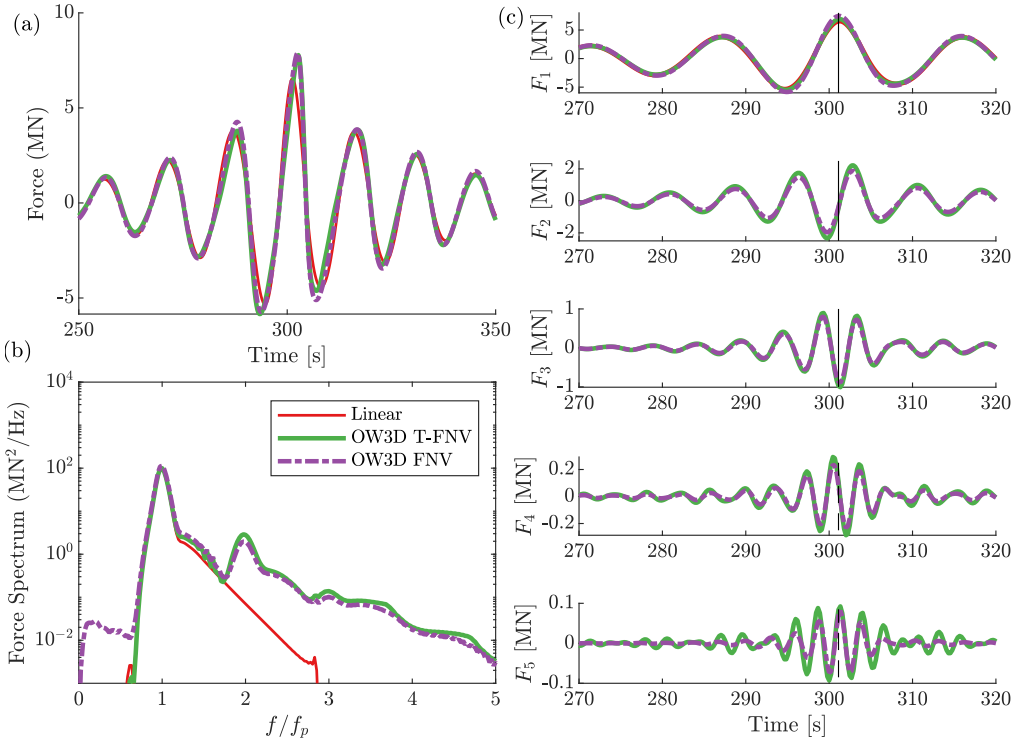

Figure 6: Comparison between the finite water depth FNV theory and the T-FNV approximations with only free-surface elevation as input for $k_p d = 1.19$ ($k_p A = 0.17$) (a): total inline force, (b): force spectrum and (c): four-phase separated higher order harmonics.

5. Discussions and conclusions

We present a transformed version of the FNV model that solely incorporates free-surface quantities. Numerical tests show satisfactory accuracy of this new formulation for wave groups on both deep water and finite water depth when compared to the original FNV formulation.

This novel approximation shows that much of the nonlinearity in the higher-order force harmonics is associated with nonlinear contributions to the horizontal velocity over water depth at the column, so resides within the first depth integral term $\int_{-d}^{\eta} \frac{\partial}{\partial t} u \mathrm{d}z$. The progressive coefficient in front of each order (i.e., $1\eta_1 + 2\eta_2 + 3\eta_3 ... \mathrm{n}\,\eta_\mathrm{n}$) shows the growing importance of higher harmonics in force calculations. This also shows that the dominant force contribution can be approximated through terms with a similar form to the local wave slope in time, which would allow potential application to any wave free surface without discontinuities in value – even the Stokes 120° limiting crest shape which would produce a jump in force as the sharp crest passes.

Additionally, the new T-FNV formulation also suggests the total contribution of the last two terms $\int_{-d}^{\eta(t)} u \frac{\partial u}{\partial x} \mathrm{d}z + \int_{-d}^{\eta(t)} 2w \frac{\partial u}{\partial z} \mathrm{d}z$ is relatively small, and comes close to vanishing for $k_p d \approx 0.88$, indicating the formulation

$$F = 2\rho\pi R^2 \ \left(-g \tanh(k_p d) \left\{\eta_1 + 2\eta_2 + 3\eta_3 + \cdots\right\}_H - u_s \eta_t\right) + F^{\psi}_{\mathrm{FNV}} \quad (33)$$

would still provide satisfactory total inline force predictions.

We would also like to point out one limitation of the fully nonlinear form of the current T-FNV model, where for experimental measurements, the proposed method requires the separation of higher-order harmonics from the fully nonlinear free-surface elevation records. Four repeats of the experiments or numerical simulations are usually required with different wave phases to separate these higher-order harmonics (see Fitzgerald et al. (2014); Feng et al. (2020)). With additional approximations, this requirement can be dropped: The FNV 3rd order point load term $\sim u^2 \partial u/\partial t$ can be adequately modelled using $\sim \eta_1^2 \partial \eta_1/\partial t$, and at frequencies around the 3rd harmonic η_1 and the fully nonlinear η can be used interchangeably.

In summary, we show how the entire FNV force time history on a uniform and vertical compact cylinder can be accurately approximated based only on the fully nonlinear free-surface elevation time history, measured or calculated at the position of the column but in its absence.

Appendix A. Shallow water correction for T-FNV on characteristic wave period

We report an improved level of agreement between the proposed T-FNV and the original FNV formulation for the 2nd to 4th harmonics through an empirical shallow water correction on the characteristic wave period. Previously we assumed that T_p, the peak of the spectral energy density was suitable. For the relatively shallow water cases, we find that a single correction as a function of $k_p d$ on the characteristic wave period T_p can further improve the agreement on higher-order force harmonics. The coefficients are shown in Table A.1. We still use the finite depth linear dispersion equation to relate corrected characteristic wave period to frequency and then wavenumber (so both characteristic frequency and the characteristic wavenumber are corrected accordingly). And we note that the phasing of the every individual harmonic component of the entire force structure is unaltered by this change.

Table A.1: Shallow water correction as a function of $k_p d$ on the characteristic wave period T_p for fully approximated T-FNV.

ine **Relative Water Depth** ($k_p d$)	$k_p d = 0.88$	$k_p d = 1.19$	$k_p d = 3.39$
ine **Correction on** T_p	$1.14T_p$	$1.09T_p$	$1.01T_p$
ine			

In Figure A.7, A.8 and A.9, we present the comparison between finite water depth FNV theory and the shallow water corrected T-FNV approximation. The modified T-FNV model now shows much improved agreement with the finite water depth FNV theory. Further studies are required to investigate this correction to determine the full expression form to see if there is any theory to support it or if it remains a useful empirical correction, and to assess the overall merit of using it when T-FNV is applied to random waves using Monte Carlo techniques. This will be reported in a follow-on paper.

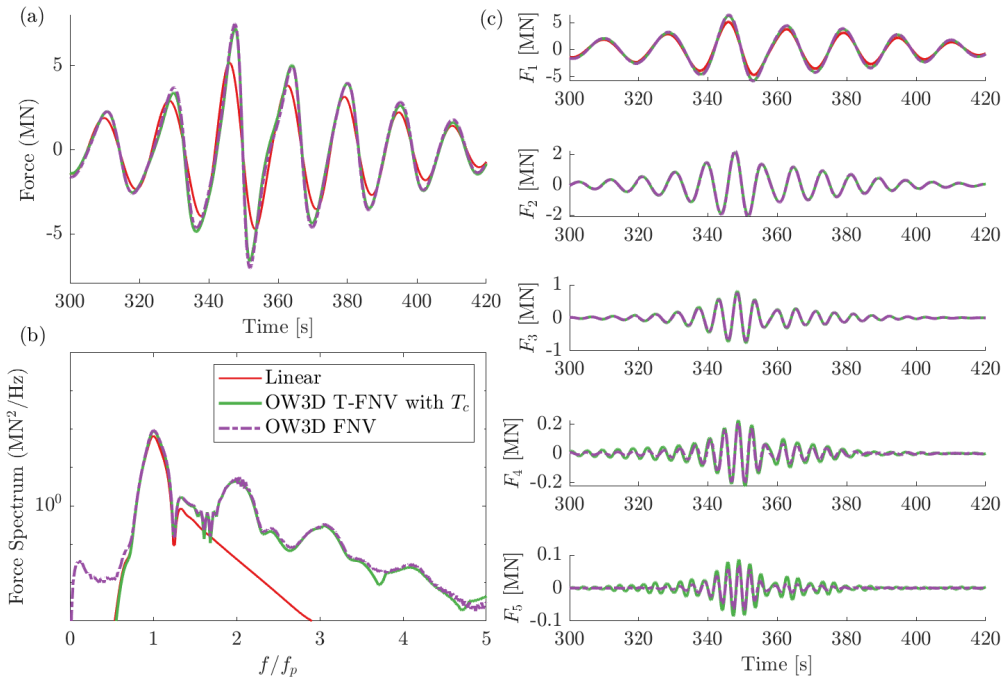

Figure A.7: Comparison between the finite water depth FNV theory and full T-FNV approximations with shallow water corrected characteristic wave period(see Table A.1) for the case with $k_p d = 0.88$ ($k_p A = 0.17$): total inline force, (b): force spectrum and (c): four-phase separated higher order harmonics.

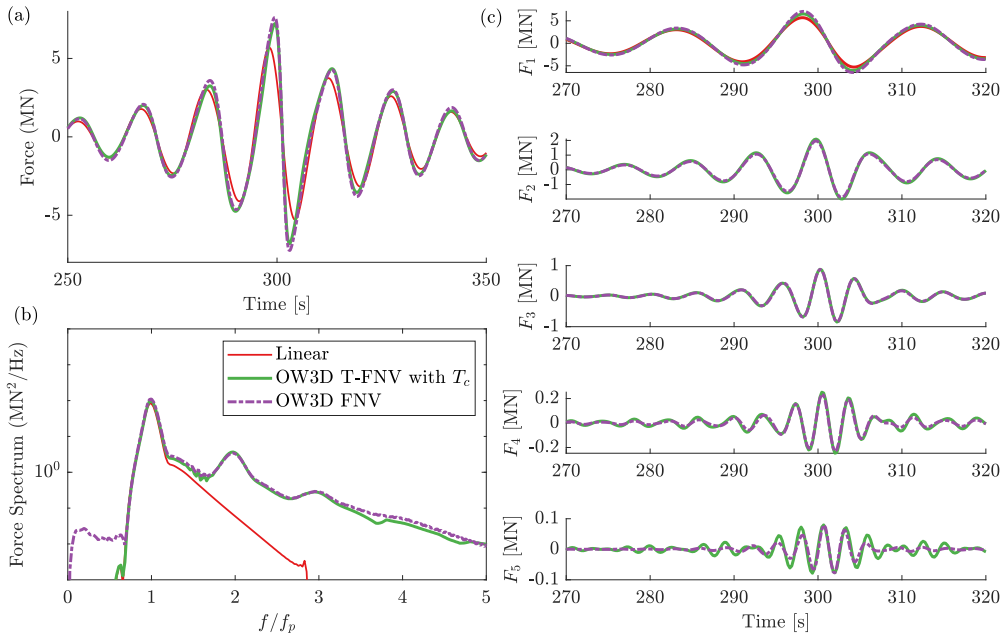

Figure A.8: Comparison between the finite water depth FNV theory and full T-FNV approximations with shallow water corrected characteristic wave period(see Table A.1) for the case with $k_p d = 1.19$ ($k_p A = 0.17$): total inline force, (b): force spectrum and (c): four-phase separated higher order harmonics.

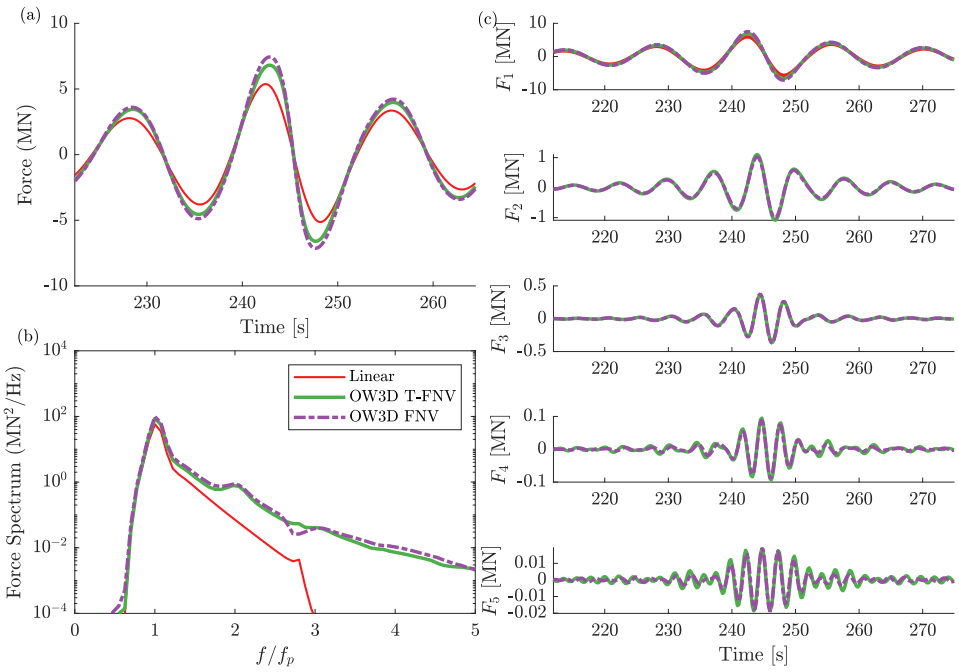

Figure A.9: Comparison between the finite water depth FNV theory and full T-FNV approximations with shallow water corrected characteristic wave period(see Table A.1) for the case with $k_p d = 3.39$ ($k_p A = 0.17$): total inline force, (b): force spectrum and (c): four-phase separated higher order harmonics.

Acknowledgement

TT is funded by an Eric and Wendy Schmidt AI in Science Postdoctoral Fellowship. TT would also like to acknowledge the Robert and Maude Gledden Short Stay Visiting Fellowship, funded by the University of Western Australia, and the TIDE Project (the ARC ITRH for Transforming energy Infrastructure through Digital Engineering (TIDE, http://TIDE.edu.au) Grant No. IH200100009) for funding his visit to UWA. This research was funded in whole or in part by EPSRC grant number EP/V050079/1. For the purpose of Open Access, the author has applied a CC BY public copyright licence to any Author Accepted Manuscript (AAM) version arising from this submission. We thank Profs. John Grue (University of Oslo) and Trygve Kristiansen (Norwegian University of Science and Technology) for their technical advice.

References

Baldock, T.E., Swan, C., Taylor, P.H., 1996. A laboratory study of nonlinear surface waves on water. Philos. Trans. Royal Soc. A Math. Phys. Eng. Sci. 354, 649–676.

Barratt, D., Bingham, H.B., Adcock, T.A.A., 2020. Nonlinear evolution of a steep, focusing wave group in deep water simulated with OceanWave3D. J. Offshore Mech. Arct. Eng. 142, 021201.

Birkhoff, G., Kreyszig, E., 1984. The establishment of functional analysis. Historia Mathematica 11, 258–321.

Calvert, R., Whittaker, C., Raby, A., Taylor, P.H., Borthwick, A., Van Den Bremer, T., 2019. Laboratory study of the wave-induced mean flow and set-down in unidirectional surface gravity wave packets on finite water depth. Phys. Rev. Fluids. 4, 114801.

Chen, L.F., Zang, J., Taylor, P.H., Sun, L., Morgan, G.C.J., Grice, J., Orszaghova, J., Ruiz, M.T., 2018. An experimental decomposition of nonlinear forces on a surface-piercing column: Stokes-type expansions of the force harmonics. J. Fluid Mech. 848, 42–77.

Eatock Taylor, R., Hung, S.M., 1987. Second order diffraction forces on a vertical cylinder in regular waves. Appl. Ocean Res. 9, 19–30.

Engsig-Karup, A.P., Bingham, H.B., Lindberg, O., 2009. An efficient flexible-order model for 3D nonlinear water waves. J. Comput. Phys. 228, 2100–2118.

Faltinsen, O.M., Newman, J.N., Vinje, T., 1995. Nonlinear wave loads on a slender vertical cylinder. J. Fluid Mech. 289, 179–198.

Feng, X., Taylor, P.H., Dai, S., Day, A.H., Willden, R.H.J., Adcock, T.A.A., 2020. Experimental investigation of higher harmonic wave loads and moments on a vertical cylinder by a phase-manipulation method. Coast. Eng. 160, 103747.

Fenton, J.D., 1990. Nonlinear wave theories, in The Sea, Vol.9: Ocean Engineering Science. volume 9. Wiley, New York.

Fitzgerald, C.J., Taylor, P.H., Eatock Taylor, R., Grice, J., Zang, J., 2014. Phase manipulation and the harmonic components of ringing forces on a surface-piercing column. Proc. R. Soc. A: Math. Eng. Sci 470, 20130847.

Huseby, M., Grue, J., 2000. An experimental investigation of higher-harmonic wave forces on a vertical cylinder. J. Fluid Mech. 414, 75–103.

International Electrotechnical Commission, 2009. 61400-3, Wind turbines-part 3: Design requirements for offshore wind turbines. IEC, Geneva .

Kristiansen, T., Faltinsen, O.M., 2017. Higher harmonic wave loads on a vertical cylinder in finite water depth. J. Fluid Mech. 833, 773–805.

Malenica, Š., Clark, P.J., Molin, B., 1995. Wave and current forces on a vertical cylinder free to surge and sway. Appl. Ocean Res. 17, 79–90.

Mj, D., McAllister, M.L., Bredmose, H., Adcock, T.A.A., Taylor, P.H., 2023. Harmonic structure of wave loads on a surface piercing column in directionally spread and unidirectional random seas. J. Ocean Eng. Mar. Energy. , 1–19.

Molin, B., 1979. Second-order diffraction loads upon three-dimensional bodies. Appl. Ocean Res. 1, 197–202.

Nestegård, A., Ronæss, M., Hagen, Ø., Ronold, K.O., Bitner-Gregersen, E.M., 2006. New DNV Recommended Practice DNV-RP-C205 On Environmental Conditions And Environmental Loads.

Newman, J.N., 1996. Nonlinear scattering of long waves by a vertical cylinder. Wave Nonlinear Process Hydrodyn. , 91–102.

Rainey, R.C.T., 1995. Slender-body expressions for the wave load on offshore structures. Proc. R. Soc. A Math. Phys. Eng. Sci. 450, 391–416.

Schløer, S., Bredmose, H., Bingham, H.B., 2016. The influence of fully nonlinear wave forces on aero-hydro-elastic calculations of monopile wind turbines. Mar. Struct. 50, 162–188.

Sharma, J.N., Dean, R.G., 1981. Second-order directional seas and associated wave forces. Soc. Pet. Eng. J. 21, 129–140.

Stokes, G.G., 1847. On the theory of oscillatory waves. Trans. Cam. Philos. Soc. 8, 441–455.

Walker, D.A.G., Taylor, P.H., Eatock Taylor, R., 2004. The shape of large surface waves on the open sea and the Draupner New Year wave. Appl. Ocean Res. 26, 73–83.

Wang, S., Larsen, T.J., Bredmose, H., 2021. Ultimate load analysis of a 10 MW offshore monopile wind turbine incorporating fully nonlinear irregular wave kinematics. Mar. Struct. 76, 102922.

Wheeler, J.D., 1970. Method for calculating forces produced by irregular waves. J. Pet. Technol. 22, 359–367.